COBEM 2021 26th International Congress of Mechanical Engineering
November 22-26, 2021, Virtual Congress, Brazil

COB-2021-2137
CORROSION RESISTANCE OF COLD-DRAWN ZK60A MG-ALLOY AS A FUNCTION OF STRAIN-HARDENING

Pedro Brito
Thais Roberta Campos
Beatriz Paulinelli Ferreira
Pontifical Catholic University of Minas Gerais, Graduate Program in Mechanical Engineering (PPGEM), Av. Dom José Gaspar 500, Belo Horizonte (MG) 30535-901, Brazil.
pbrito@pucminas.br, trcampos@sga.pucminas.br, beatrizpaulinelli@gmail.com

Diogo Azevedo de Oliveira
Federal University of Minas Gerais, Graduate Program in Mechanical Engineering (PPGMEC), Av. Presidente Antônio Carlos 6627, Belo Horizonte (MG) 31270-901, Brazil.
diogoazev@yahoo.com.br

Klaus Higor dos Santos Silva
Jonathan Mendes das Chagas Crosara
Pontifical Catholic University of Minas Gerais (Liberty Square), Mechanical Engineering, R. Claudio Manoel 1162, Belo Horizonte (MG) 30140-002, Brazil.
klaushigor@pucminas.br, jonathanmendes8028@gmail.com

Rodrigo Santiago Coelho
SENAI-CIMATEC, Institute of Innovation for Forming and Joining of Materials, Av. Orlando Gomes 1845, Salvador (BA) 41650-010, Brazil
rodrigo.coelho@fieb.org.br

Abstract. *Magnesium alloys exhibit elevated strength to weight ratio, high capacity for absorbing mechanical vibrations as well as good machinability and castability. One of the main disadvantages of magnesium alloys is their elevated chemical reactivity, which might limit application in certain media or impose protective measures. As such, efficient and safe use of magnesium alloys requires an understanding of their corrosion resistance in relation to previous processing/microstructure conditions which might influence electrochemical behavior. In the present work, an exploratory work of the corrosion resistance of magnesium alloy ZK60A (0.5%Zr and 5.5%Zn) in 3.5%NaCl solution containing naturally dissolved oxygen was performed. Tests were performed on samples in the T5 (aged) condition and submitted to different levels of cold-work by drawing in order to evaluate the relation between strain-hardening and corrosion behavior. To this end, mechanical properties of the samples (tensile test and hardness) and microstructure (crystallographic texture). The corrosion resistance was evaluated by means of electrochemical impedance spectroscopy and potentiodynamic polarization. The results obtained revealed that the drawing process causes the (10-10) planes to become perpendicular to the drawing direction, as opposed to the initially randomly textured samples in the T5 condition. The corrosion resistance could was found to be dependent on the level of strain-hardening, with a small increase in corrosion rate as a function of cold-work.*

Keywords: *Magnesium alloy, cold-drawing, crystallographic texture, corrosion resistance, strain-hardening.*

1. INTRODUCTION

Magensium alloys are currently comprise some of the lightest density metals used in structural applications. These materials exhibit good strength to weight ratio, excellent vibration damping capacity and have good castability. For these reasons, Mg-alloys have been increasingly considered as possibilities for reducing weight in the automotive and aerospace industries (Froes *et al*., 1997). Some of the difficulties associated with Mg-alloys involve reduced thickness, low toughness and formability, low creep resistance and elevated reactivity (Mordike and Ebert, 2000).

The relatively low performance of Mg-alloys in forming processes (compared to other metals, such as Al-alloys) is attributed to the HCP close-pack structure which presents limited slip systems at low temperature (Koike, *et al*., 2003). Additionally, forming processes induce strong crystallographic textures in wrought Mg-alloys (Gall *et al*., 2013; Chen *et al*., 2015; Li *et al*., 2018), and texture analyses of products obtained by hot or cold forming processes are important for the assessment mechanical properties and overall performance (Wang, *et al*., 2018; Lloyd *et al*., 2019).

From investigations of the electrochemical behavior of Mg-alloy single crystals, it is known that atomic packing plays an important role in corrosion resistance, with more densely occupied crystal planes exhibiting lower corrosion rates (Hagihara *et al*., 2016). Therefore, it is important to consider the relation between texture and microstructure modifications induced by forming processes on the corrosion behavior of Mg-alloys. Currently, most investigations have focused extrusion (Mostaed, *et al*., 2014; He, *et al*., 2017) and sheet-forming processes (Gu, *et al*., 2009; Xin *et al*., 2011), with relatively less information available concerning other common forming operations such as drawing.

In the present work, the corrosion resistance of Mg-alloy ZK60A as a function of deformation in cold-drawing was investigated. The objective of this research is to assess the extent to which alterations in crystallographic may modify the electrochemical behavior of the selected material in a neutral Cl^- environment.

2. EXPERIMENTAL PROCEDURE

2.1 Cold-drawing process and mechanical properties

The materials used in the present investigation were ZK60A Mg-alloy (5.5%Zn, 0.5%Zr) round bars initially received in the aged condition (T5 treatment), supplied by Metalmart Intarnational Inc (USA). The initial 25mm diameter was reduced in successive drawing operations to 24, 23, 22 and 21 mm which resulted in cold-work values of 7.8, 15.4, 22.6 and 29.4%, respectively, as in previous investigations (Oliveira *et al*., 2014; Silva *et al*., 2014). The mechanical behavior of the cold-drawn bars was evaluated after each deformation step by submitting the materials by conventional tensile tests performed in EMIC DL20000 equipment. The tensile tests were performed according to the ABNT NBR 6152 (2002) standard at a strain rate of 0.04 min^{-1}. All mechanical tests were performed three times for reproducibility.

2.2 Crystallographic texture analysis

Crystallographic texture analysis on as received and cold-drawn samples were performed by X-Ray Diffraction (XRD). The tests were performed using a laboratory source operating with Cu K_α radiation. XRD spectra were collected within a diffraction angle (2θ) range of 25 to 65°, which allowed acquisition of reflections from the (100), (002), (101), (102) and (110) planes, located at 2θ positions of 32.25, 34.45, 36.65, 47.9 and 57.45°. The samples were rotated around the azimuthal angle from 0 to 360° in 5° steps and were tilted from 0 to 85° also in 5° steps. The data acquired was then processed using MTEX software for generating graphical representations of the experimentally determined pole figures. The samples submitted to texture were evaluated on their cross-section, *i.e.* the perpendicular to the drawing direction.

2.3 Corrosion resistance

Selected cold-drawn samples were submitted to corrosion testing in order to verify whether the incremental drawing process could lead to a change in corrosion resistance. The tests were performed in 0.6M NaCl aqueous solution (3.5wt.%) in a 500 ml flat cell with a 10.0 mm diameter orifice for exposing the sample surface to the electrolyte. The surfaces of the samples were prepared by grinding and polishing with a diamond suspension down to a 1 μm finish. A three-electrode setup was used, with a platinum wire counter electrode, Ag/AgCl reference electrode and the Mg-alloy samples as work electrode. Initially, the Open Circuit Potential (OCP) was monitored for 3600 s to allow for stabilization. Subsequently, Electrochemical Impedance Spectroscopy (EIS) analyses were performed at the stabilized OCP value by applying a 0.01 V amplitude sinusoidal signal with frequencies varying between 100,000 and 0.01 Hz. Finally, potentiodynamic polarization scans were performed from -1.8 to 0.8V in 1mV steps and 2mV/s scan rate. The polarization data was used to obtain corrosion potential (E_{corr}) and corrosion current density (i_{corr}) by modeling the experimental curves with the Butler-Volmer equation (1):

$$i = i_{\text{corr}}\left[e^{\frac{2.303(E-E_{\text{corr}})}{b_C}} - e^{\frac{2.303(E-E_{\text{corr}})}{b_A}}\right] \quad (1)$$

where i is the current density, E is the applied electrode potential, b_C is the cathodic Tafel slope and b_A is the anodic Tafel slope. The electrochemical tests were performed three times on the analyzed samples, for reproducibility.

3. RESULTS AND DISCUSSION

3.1 Mechanical properties

The results obtained from the tensile tests as a function of drawing reduction are presented in Figure 1, which summarizes the variation of tensile strength and ductility as a function of drawing reduction for the as received and 7.8, 15.4, 22.6 and 29.4% cold worked samples. As expected, with an increase in prior deformation, the ZK60A alloy experienced an increase in tensile strength and a decrease in ductility, caused by strain-hardening.

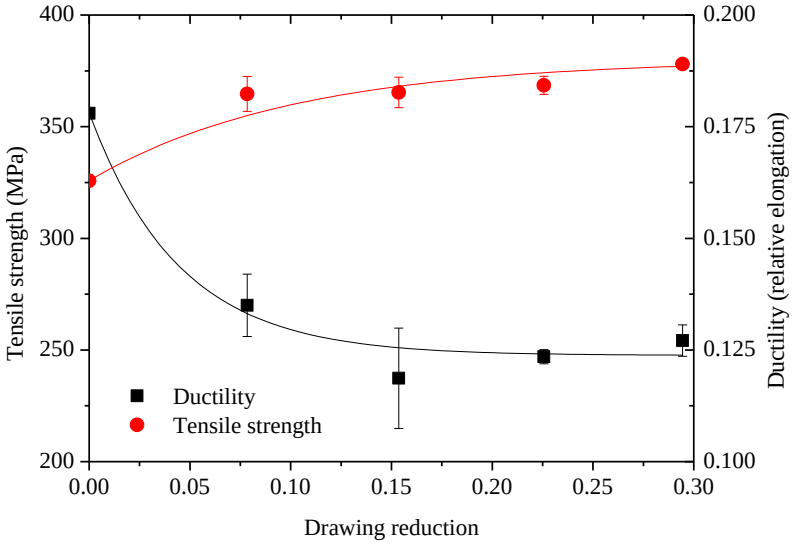

Figure 1. Schematic diagram of the control strategy.

3.2 Crystallographic texture analysis

The experimental pole figures determined for the different ZK60A samples are presented in Figure 2(a-d). In each case, texture strength is indicated by multiples of a random distribution (m.r.d). It is possible to notice that initially, the T5-aged samples exhibit an approximately random texture distribution, with a low maximum texture strength (3.3 m.r.d) and no particularly strong texture components.

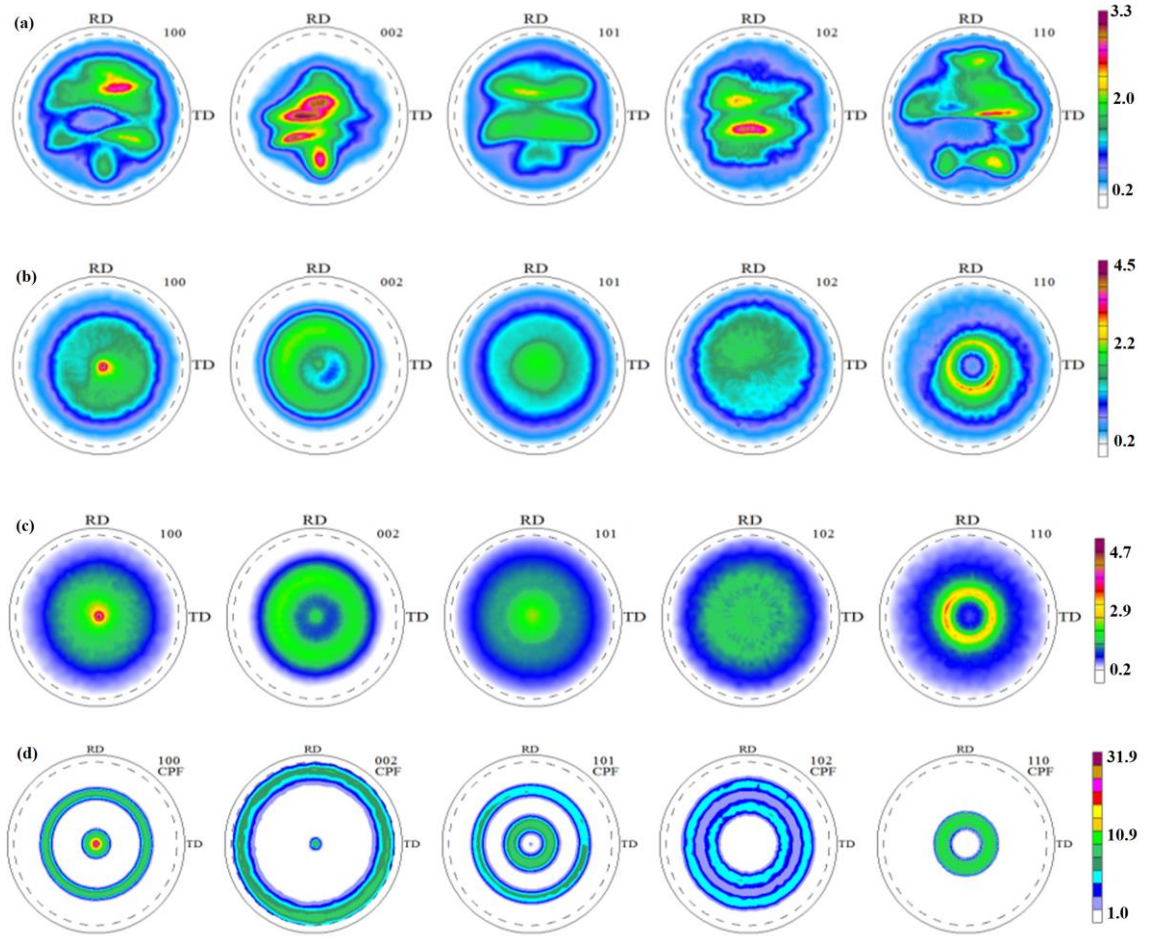

Figure 2. Pole figures determined for the (a) as-received (T5), (b) 7.8%CW, (c) 22.6%CW and (d) 29.4%CW samples.

With the drawing process, the presence of crystallographic texture can be discerned, for the lower values of reduction, but texture strength is still low (at 7.8 and 22.6%CW the maximum texture strengths of 4.5 and 4.7, respectively). By analyzing the (100) and (002) pole figures shown in Figures 2(b) and 2(c), it is possible to notice that the prismatic (100) planes become oriented parallel to the sample surface (so normal to the drawing direction) while the basal (002) planes become are oriented along the sample radial direction. The same texture formation is observed in the subsequent reduction (29.4%), but here the texture strength increases significantly (maximum texture strength of 31.9 m.r.d). The results are in agreement with previous observations concerning the extrusion of AZ31, AZ61 and AZ81 alloys (Mueller *et al*., 2006) and the initial drawing behavior (up to 3% strain) of a Mg-2%Zn alloy (Jing-Bai *et al*., 2017) – although in the latter case, the authors noticed that upon further drawing passes the initial texture was modified.

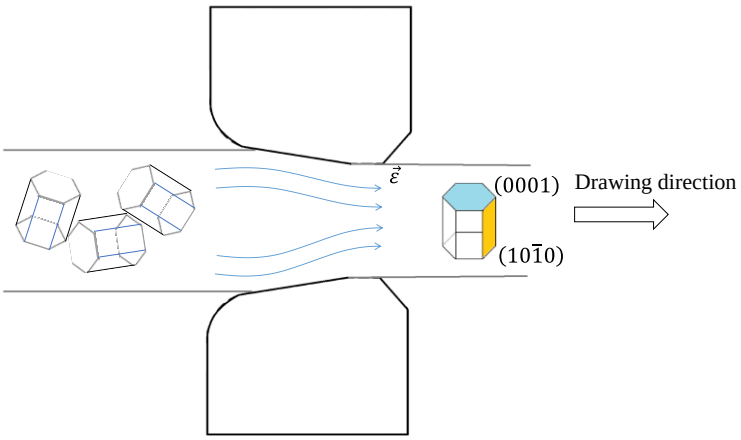

Figure 3. Schematic representation of texture formation during drawing of initially randomly oriented Mg-alloy bars leading to prismatic planes normal to the drawing direction and basal planes oriented along the sample radius.

A possible explanation for this behavior is that the deformation by slip on the HCP structure of Mg takes place on the basal (0001) plane. As such, there is tendency that the (002) planes (parallel to the basal plane) become oriented parallel to the material flow curves during deformation through the drawing die, as illustrated schematically in Figure 3. Since the flow curves follow the drawing direction, basal planes become oriented along the sample radius while the prismatic $(10\bar{1}0)$ become oriented perpendicular to the drawing direction. It remains to be investigated whether the significant increase in texture strength is connected to the fracture of the bars (by torsion) that took place during the attempt to perform subsequent drawing passes.

3.3 Corrosion behavior

Based on the information obtained concerning crystallographic texture of the cold-drawn ZK60A specimens, a series of electrochemical tests were performed with the objective of evaluating corrosion resistance. The samples selected for further examination were those in the as-received condition (random texture, low strain-hardening), and submitted to 22.6 (weak texture, strain-hardened) and 29.4%CW (strong texture, strain-hardened) samples. The evolution of OCP over time is presented in Figure 4, for the as-received, as well as 22.6 and 29.4%CW samples. It is possible to notice that after 3600 s exposure to the 0.6M NaCl solution OCP values become stabilized (with a variation of approximately 0.1mV/hour) at approximately -1.505, -1.515 and -1.525 for the T5, 22.6%CW and 29.4%CW samples, respectively.

Following OCP stabilization, EIS tests were performed and the obtained results are presented in Figure 5, in the form of Nyquist plots. The equivalent circuit model (Hagihara *et al*. 2016) used to fit the experimental data is also presented in Figure 5. The EIS results indicate the presence of a single depressed capacitive arc, which was modeled using a constant phase element with impedance (Z_{CPE}) given by (Stoynov, 1990):

$$Z_{\mathrm{CPE}} = [Q(j\omega)^n]^{-1} \qquad (2)$$

where Q is a constant and n is an adjustable factor ranging from -1 (inductive behaviour) to 1 (capacitive behaviour).

In the impedance model adopted (Figure 5), the terms R_P and Q correspond, respectively, to the charge transfer resistance and the capacitance of the electrical double layer formed at the metal/solution interface, while R_S is the impedance due to the solution. According to Hagihara *et al*. (2016), the terms R_L and L correspond to inductive behaviour (the negative Z_1 values in Figure 5) that is caused by the adsorption of Mg^+ at the metal surface. The model adopted does

not take into account the presence of an oxide film on the metal surface, which would be indicated in the experimental data by a second capacitive arc.

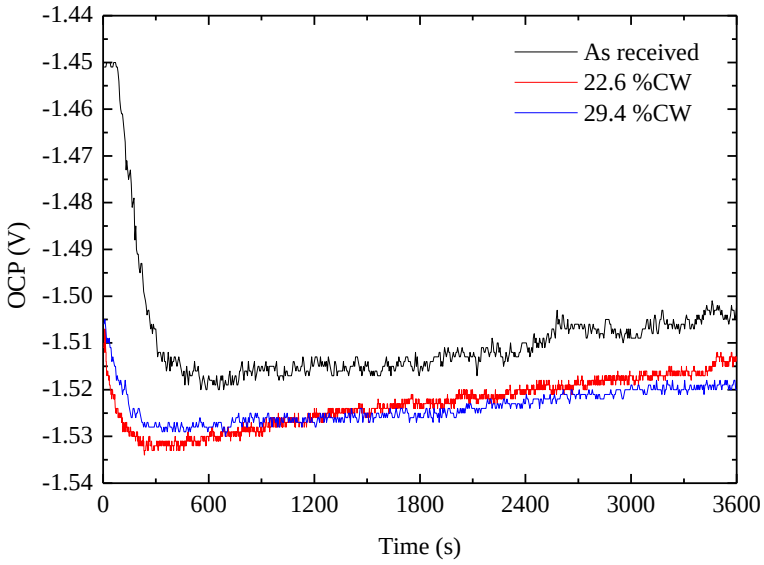

Figure 4. Open Circuit Potential (OCP) monitoring in 0.6M NaCl solution.

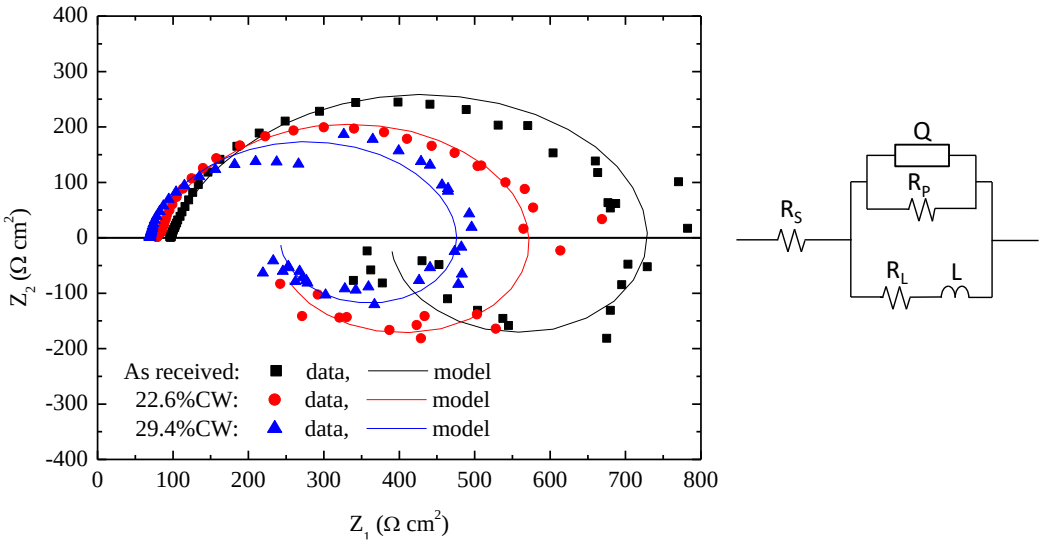

Figure 5. Nyquist diagram generated with the EIS data along with the equivalent circuit used to model the experimental data (based on Hagihara *et al*., 2016)

The results obtained from the EIS data are summarized in Table 1. Overall, for all tested materials, the charge transfer mechanisms of the freely corroding metallic surface are the same, which is indicated by the similar *Q* and *n* values. The charge transfer resistance, however, which is inversely proportional to the corrosion rate, did vary according to the tested sample. Among the three experimental conditions, largest resistance to metal dissolution was observed in the T5 condition, followed by the 22.6%CW and 29.4%CW conditions.

Table 1. Summary of the EIS data obtained for the aged and cold-drawn ZK60A Mg-alloy samples in 0.6M NaCl (fitting errors for each parameter are in parenthesis)

Sample	R_S **(Ω)**	R_P **(Ω)**	R_L **(Ω)**	Q **(×10^{-5} Fs^{n-1})**	L **(H)**	n
T5	120.5 (1.7%)	845.9 (3.81%)	643.5 (7.23%)	5.79 (11.35%)	1000 (11.61%)	0.843 (2.6%)
22.4%CW	99.5 (1.18%)	639.8 (2.13%)	276.7 (7.88%)	3.05 (8.4%)	443.8 (4.94%)	0.862 (1.63%)
29.4%CW	86.31 (1.49%)	523.6 (2.64%)	369.6 (5.98%)	4.28 (10.55%)	758.3 (8.14%)	0.882 (2.11%)

The results of the potentiodynamic polarization scans are presented in Figure 6. The samples presented a well-defined active region, but no significant passive behavior. The 22.6%CW and 29.4%CW samples exhibited a limited passive range, with transpassive potentials of approximately -1.1 and -1.05 V, respectively, but the T5 sample did not exhibit discernible passive behaviour. In the absence of passivity, the corrosion resistance of the alloys can be analyzed based on the corrosion potential (E_{corr}) and corrosion current density (i_{corr}) values, which are presented in Table 2. By considering these two parameters, it is possible to notice that with increased amount of cold-work, the samples become more reactive, which is indicated by the shift to more negative values of E_{corr} as a function of cold-work. In addition, the corrosion current density, directly linked to the materials corrosion rate, also increased with the amount of cold work. Therefore, the results obtained from the potentiodynamic polarization measurements are consistent with the EIS analyses, which showed corrosion resistance followed the order T5 > 22.6%CW > 29.4%CW.

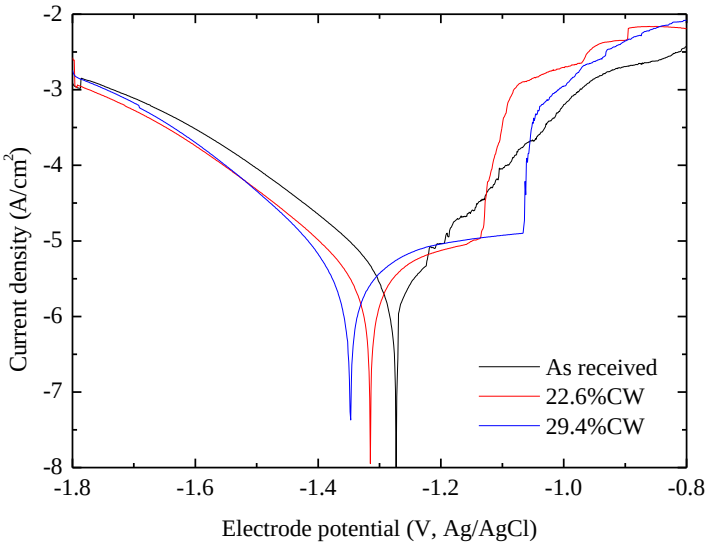

Figure 6. Potentiodynamic polarization curves obtained from T5-aged and cold-drawn ZK60A Mg-alloys in 0.6M NaCl.

Table 2. Polarization results obtained for the aged and cold-drawn ZK60A Mg-alloy samples in 0.6M NaCl.

Sample	E_{corr} (V-Ag/AgCl)	i_{corr} (μA/cm²)	b_A (V/dec)	b_C (V/dec)
T5	-1.30 ± 0.04	2.01 ± 0.83	0.09 ± 0.04	-0.11 ± 0.04
22.4%CW	-1.30 ± 0.02	3.44 ± 2.06	0.39 ± 0.09	-0.17 ± 0.02
29.4%CW	-1.37 ± 0.02	8.00 ± 4.84	0.41 ± 0.33	-0.14 ± -0.03

The crystallographic texture analyses indicates that in the T5 condition a near random texture. In this condition, the material is also in least strain-hardened condition among the samples tested in this investigation. By increasing the amount of cold work in the drawn samples, the texture was modified so that the basal planes were oriented along the bars radial direction while the $(10\bar{1}0)$ planes were perpendicular to the sample normal direction (and to a relatively larger extent in the 29.4%CW sample, that exhibited a significantly higher texture strength). The $(10\bar{1}0)$ plane of the HCP structure is, however, of average planar density. Comparing in-plane atomic densities for the (0001), $(11\bar{2}0)$, $(10\bar{1}0)$, $(11\bar{2}3)$, $(10\bar{1}2)$ gives values of 11.21, 6.91, 5.98, 2.54 and 4.09×10^{14} atoms per cm^2, respectively (Hagiara *et al*., 2016). Therefore, by increasing texture strength and increasing the amount of $(10\bar{1}0)$ planes which are exposed to the electrolyte, it can be expected that the average planar density does not deviate significantly from the nearly random texture condition (T5) or between the samples with different texture strengths (22.6%CW and 29.4%CW). In the present case, therefore, it is likely that the amount of cold work is responsible for decreasing corrosion resistance to a larger extent than the samples crystallographic texture.

4. CONCLUSIONS

In the present investigation, ZK60A-T5 Mg-alloy bars were submitted incremental cold-drawing operations up to 29.4% cold work. With each cold drawing pass, the materials exhibited an increase in mechanical strength and decrease in ductility as a consequence of strain-hardening. The initial samples, in the aged condition, exhibited a near random crystallographic texture. With the drawing process, crystallographic texture strength was increased with the c-axis of the HCP structure oriented parallel to the sample radial direction and the $(10\bar{1}0)$ planes oriented perpendicular to the drawing

direction. The corrosion behavior of the cold-drawn ZK60A alloys was found to be more influenced by the amount of strain hardening than by crystallographic texture, following the tendency: T5 > 22.6%CW > 29.4%CW.

5. ACKNOWLEDGEMENTS

This study was financed in part by the Coordenação de Aperfeiçoamento de Pessoal de Nível Superior - Brazil (CAPES) - Finance Code 001 and by the Pontifical Catholic University of Minas Gerais (FIP 1/2013-7626-S1).

6. REFERENCES

Chen, W. Z., Zhang, W. C., Chao, H. Y., Zhang, L. X., and Wang, E. D., 2015. "Influence of large cold strain on the microstructural evolution for a magnesium alloy subjected to multi-pass cold drawing". *Materials Science and Engineering: A*, Vol. 623, No. 9, pp. 92-96.

Froes, F. H., Eliezer, D., and Aghion, E. 1998. "The science, technology and applications of magnesium". *Journal of the Minerals, Metals and Materials Society*, Vol. 50, No. 9, pp. 30-34.

Gu, Z. W., Han, Y., Pan, F. S., Wang, X., Weng, D., and Zhou, S., 2009. "Effect of microstructure and texture on corrosion resistance of magnesium alloy". *Materials Science Forum*, Vol. 610-613, pp. 1160-1163.

Hagihara, K., Okubo, M., Yamasaki, M., and Nakano, T., 2016. "Crystal-orientation-dependent corrosion behaviour of single crystals of a pure Mg and Mg-Al and Mg-Cu solid solutions". *Corrosion Science*, Vol. 109, pp. 68-85.

He, J., Jiang, B., Xu, J., Zhang, J., Yu, X., Liu, B., and Pan, F., 2017. "Effect of texture symmetry on mechanical performance and corrosion resistance of magnesium alloy sheet". *Journal of Alloys and Compounds*, Vol. 723, pp. 213-224.

Jing Bai, L. S., Xue, F., Tao, L., Chu, C., and Meng, J., 2017. "Exceptional texture evolution induced by multi-pass cold drawing of magnesium alloy". *Materials & Design*, Vol. 135, pp. 267-274.

Koike, J., Kobayashi, T., Mukai, T., Watanabe, H., Suzuki, M., Maruyama, K., and Higashi, K., 2003. "The activity of non-basal slip systems and dynamic recovery at room temperature in fine-grained AZ31B magnesium alloys". *Acta Materialia*, Vol. 51, pp. 2055-2065.

Li, C.-j, Sun, H.-f., Cheng, S., Tan, H.-m, He, T.-h, and Fang, W.-b., 2018. , J., Kobayashi, T., Mukai, T., Watanabe, H., Suzuki, M., Maruyama, K., and Higashi, K., 2003. "The activity of non-basal slip systems and dynamic recovery at room temperature in fine-grained AZ31B magnesium alloys". *Acta Materialia*, Vol. 51, pp. 2055-2065.

Lloyd, J. T., Matejunas, A. J., Becker, R., Walter, T. R., Priddy, M. W., and Kimberly, J. 2019. "Dynamic tensile failure of rolled magnesium: Simulations and experiments quantifying the role of texture and second-phase particles". *International Journal of Plasticity*, Vol. 114, pp. 174-195.

Mordike, B. L., and Ebert, T., 2001 "Magnesium – Properties – Applications – Potential". *Materials Science & Engineering A*, Vol. 302, pp. 37-45.

Mostaed, E., Hashempour, M., Fabrizi, A., Dellasega, D., Bestetti, M., Bonollog, F., and Vedani, M., 2014. "Microstructure, texture evolution, mechanical properties and corrosion behavior of ECAP processed ZK60 magnesium alloy for biodegradable applications". *Journal of the Mechanical Behavior of Biomedical Materials*, Vol. 37, pp. 307-322.

Mueller, S., Mueller, K., Tao, H., and Reimers, 2006. "Microstructure and mechanical properties of the extruded Mg-alloys AZ31, AZ61, AZ80". International Journal of Materials Research, Vol. 97, No. 10, pp. 1384-1391.

Oliveira, D. A., Silva, K. H. S., Silva, G. C., and Brito, P., 2014. "Propriedades mecânicas e recristalização estática da liga de magnésio ZK60A conformada a frio por trefilação". In: *Anais do 69º Congresso Anual da ABM - Internacional*. São Paulo, Brazil.

Silva, K. H. S., Cunha, R. B., Oliveira, D. A., Silva, G. C., and Brito, P. P., 2014. "Cold-drawing behavior of magnesium alloy ZK60A round bars". In: *Anais do 8º Congresso Nacional de Engenharia Mecânica – CONEM 2014*, Uberlândia, Brazil.

Stoynov, Z., 1990. "Impedance modeling and data processing: structural and parametrical estimation". *Electrochimica Acta*, Vol. 35, pp. 1493-1499.

Xi, R., Li, B., Li, L., and Liu, Q., 2011. "Influence of texture on corrosion rate of AZ31 Mg alloy in 3.5 wt.% NaCl". *Materials & Design*, Vol. 32, No. 8-9, pp. 4548-4552.

Wang, W., Ma, L., Chai, S., Zhang, W., Chen, W., Feng, Y., and Cui, G. 2018. "Role of one direction strong texture in stretch formability for ZK60 magnesium alloy sheet". *Materials Science and Engineering: A*, Vol. 730, pp. 162-167.

7. RESPONSIBILITY NOTICE

The authors are the only responsible for the printed material included in this paper.